Onset and Saturation of Ion Heating by Odd-Parity Rotating Magnetic Fields in a Field-Reversed Configuration

A. S. Landsman,[1,*] S. A. Cohen,[2] and A. H. Glasser[3]
[1]*Naval Research Laboratory, Washington, Distrct of Columbia, USA*
[2]*Princeton Plasma Physics Laboratory, Princeton University, Princeton, New Jersey, USA*
[3]*Los Alamos National Laboratory, Los Alamos, New Mexico, USA*
(Received 23 August 2005; published 3 January 2006)

Heating of figure-8 orbit ions by odd-parity rotating magnetic fields (RMF_o) applied to an elongated field-reversed configuration (FRC) is investigated. The largest energy gain occurs at resonances ($s \equiv \omega_R/\omega$) of the RMF_o frequency, ω_R, with the figure-8 orbital frequency, ω, and is proportional to s^2 for *s-even* resonances and to s for *s-odd* resonances. The threshold for the transition from regular to stochastic orbits explains both the onset and saturation of heating. The FRC magnetic geometry lowers the threshold for heating below that in the tokamak by an order of magnitude.

DOI: 10.1103/PhysRevLett.96.015002 PACS numbers: 52.50.Qt, 05.45.−a, 52.55.Lf, 52.65.Cc

Heating, i.e., stochastic energy gain, of charged particles by time-varying fields is a complex and fundamental phenomenon critically important to as diverse areas of plasma physics as fusion research [1] and plasma processing [2]. Well-known are the effects of simple resonances and particle collisionality on the heating of magnetized plasmas. Far less well explored is the role of an inhomogeneous static magnetic-field geometry. Because of its relevance to space plasmas [3], plasma processing [4], and magnetic-confinement controlled-fusion research [5], the field-reversed configuration (FRC) (see Fig. 1)—with its poloidal field nulls, lack of toroidal field, and strong field gradients—is an important system in which to explore the effects of magnetic-field geometry on particle dynamics under the influence of time-varying fields.

Even with axial symmetry, a static FRC allows charged-particle orbits that are regular or ergodic [6,7]. First studies of single-particle orbits in FRCs assumed time invariance and spatial symmetries that reduced the problem to one or two dimensions, allowing Kolmogorov-Arnold-Mosher (KAM) surfaces to exist [8] and limiting excursions in phase space. The addition of a rotating magnetic field (RMF) [9] breaks the angular invariance of the FRC, creating a three-dimensional system without bounding KAM surfaces and opening the possibility for large excursions in phase space and energy. These excursions can have beneficial results, such as ion heating [10,11], or detrimental ones, such as loss of confinement. In this Letter we present studies of ion orbits in FRCs with RMF applied: the goal is to understand the threshold for chaos and the role of resonances in the nonlinear growth and subsequent saturation of ion energy. We restrict attention to the novel odd-parity RMFs (RMF_o) because of field closure [12] and encouraging recent experimental results [13]. We show that the same mechanism is responsible for the initial ion heating and its ultimate saturation.

Studies of stochastic ion heating by perpendicularly propagating electrostatic waves in tokamaks were performed with similar Hamiltonian techniques and research goals [14,15]. The results we report are markedly different because of fundamental differences in the magnetic-field geometry of the two devices.

Earlier papers [10,11], which used the RMF numerical code to investigate RMF_os applied to FRCs, showed that the relevant frequency range for ion heating was broad, $|\Omega| \sim 0.2$–2, where $\Omega \equiv \omega_R/\omega_{\mathrm{ci}}$, ω_R is the RMF_o frequency, $\omega_{\mathrm{ci}} = qB_a/mc$ is the ion-cyclotron frequency in the axial field at the FRC's center, B_a, m is the ion mass, and q is the ion charge. These papers reported significant ion heating even for low relative RMF amplitude, B_R: $B_R/B_a \sim 5 \times 10^{-4}$. Phase decoherence of ion orbits, with respect to the periodic electric fields created by the RMF_o, is a necessary condition for ion heating. Strong gradients and regions of field reversal in the FRC provide locations for possible phase decoherence. For a 10 cm FRC having an ion density of 10^{14} cm^{-3} and an ion energy of 100 eV, Coulomb collisions will be 10 times less frequent than the stochastic effects described herein [10].

The question arose whether, in spite of the existence of strong field gradients, ion-cyclotron resonances (ICRs) were important to ion heating. We show that ICRs are important, but with significant differences from the standard ICR picture. More rapid heating occurs at low B_R/B_a for figure-8 orbits [see Fig. 1(b)] than for cyclotron orbits,

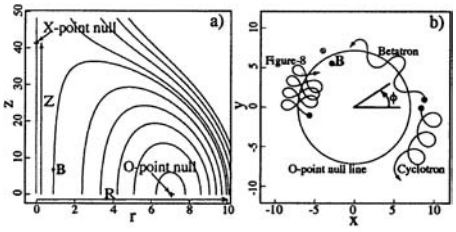

FIG. 1. (a) Shape of FRC magnetic field in z-r plane, $\kappa = 4.1$. (b) Shapes of typical cyclotron, betatron, and figure-8 orbits in $z = 0$ plane.

though the latter have a more clearly resonant interaction with RMF_o. Figure-8 orbits cross the field-reversal and strong-gradient regions (twice) every orbit cycle, possibly losing phase coherence at each traversal. In contrast, cyclotron orbits may only incur phase decoherence at the less frequent excursions to the axial extremes of their orbits. Betatron orbits have a less nonlinear nature and hence are also less well heated than figure-8 orbits. Because figure-8 orbits are representative of a large fraction of ions in hot fusion FRC plasmas and because they represent the physically interesting situation of motion in a double potential well [16], we focus on them. The studies presented herein also clarify why high-energy orbits tend to interact regularly with RMF_o, leading, importantly, to a saturation of ion heating by RMF_o and a method for tuning ion energy.

We follow Ref. [11] by using the same equations for the RMF_o and a Solov'ev equilibrium for the FRC, with the notation [see Fig. 1(a)]: R = FRC separatrix radius in midplane; Z = FRC axial half length; $\kappa \equiv Z/R$, FRC elongation; r is the radial coordinate; z is the axial coordinate; ϕ is the azimuthal coordinate; p_i are canonical momenta; $P \equiv 2p_\phi/qB_aR^2$, normalized p_ϕ; $\vec{A}$ is the vector potential of RMF and FRC; $\psi = \phi - \omega_R t$; $k = l\pi/\kappa R$ is the axial wave number of the RMF_o; l is the axial mode number; and τ is time, in units of $2\pi/\omega_{ci}$.

The shape of the effective potential-energy surface on which an ion moves depends on P and z [17]: figure-8 orbits may be confined to the $z = 0$ subspace, or to a potential-well minimum above or below $z = 0$, or may oscillate across $z = 0$. Orbits confined to the $z = 0$ subspace are amenable to an analytic analysis and are the appropriate choice to analyze because of the RMF_o's electric fields, $\mathcal{E}_r$ and $\mathcal{E}_\phi$, there. Each cross section in z is either a double potential well, allowing both cyclotron and figure-8 orbits, or a raised potential, corresponding to betatron orbits. Cyclotron orbits feel a force towards larger $|z|$, thus eventually enter a region where the barrier between the double wells is low enough for them to traverse, thereby becoming figure-8 orbits. Since cyclotron orbits interact regularly with RMF, except at these axial extremes, their random fluctuations in energy appear less frequently than for orbits which are always figure-8 shape. Moreover, figure-8 orbits have greater radial excursions, hence gain more energy from the radial electric field of the RMF_o. It follows that the heating of figure-8 orbits is an upper limit for the heating of all ions in the FRC and that the threshold for heating is highest in the $z = 0$ subspace. Extensive numerical simulations supported this.

We first examined whether the broad Ω range for heating is due to resonances at the fundamental ICR frequency. As described below, the answer is no. Instead high-harmonic resonances occur because the frequency of the figure-8 orbit is highly nonlinear. (High-harmonic resonances have recently been observed in an RMF experiment [18].) As the energy of a figure-8 orbit decreases, the ratio $s \equiv \omega_R/\omega$ increases because the ion's frequency, ω, slows down as it gets closer to the phase-space separatrix created by the hump in the double potential well. A set of resonances with the RMF_o occurs at integral values of s.

Figure 2(a) shows the RMF-code-calculated time dependence of ion energy for two values of B_R for a 1 keV ion initiated in a figure-8 orbit with zero axial velocity in the $z = 0$ subspace of a FRC having $R = 10$ cm, $\kappa = 5$, $\Omega = 0.9$, and $B_a = 20$ kG. Regular motion, with a clear $s = 5$ component, is seen for $B_R = 2$ G. The energy fluctuations are small ($\sim 15\%$) for $B_R = 2$ G and large, >100%, for $B_R = 20$ G. For $B_R = 2$ G, the fast Fourier transform (FFT) of ion energy, Fig. 2(b), shows sharp peaks in frequency space, indicative of regular motion. The separation between peaks, Δf, is 0.207 ± 0.002, in units of ω_{ci}. For $B_R = 20$ G, the FFT shows broadband noise at a 30 times higher absolute level. Under these conditions, betatron [also shown in Fig. 2(b)] and cyclotron orbits (not shown) display regular motion—sharp peaks in their FFTs—with energy fluctuations less than 7%, even for $B_R = 20$ G. Figure 2(c) shows Δf vs $\tilde{E}$, initial energy normalized to $E_n \equiv q^2B_a^2R^2/2m$, for three values of initial P and low B_R. Below $P = 0.25$ orbits may be cyclotron or figure 8; above $P = 0.25$ orbits are betatron. A logarithmic drop in Δf is seen for $P = 0.1$ and 0.2 at an energy corresponding to the phase-space separatrix energy, at the

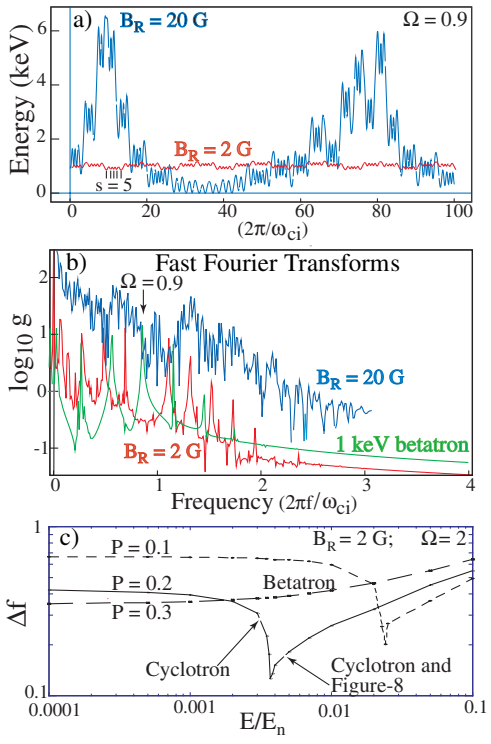

FIG. 2 (color). Results of numerical simulation of ion trajectories in a FRC with RMF_o. (a) Figure-8 ion energy vs time for two values of B_R. (b) FFTs of ion energy for the two cases shown in (a) and also for a betatron orbit. (c) Separation between resonances, Δf, vs normalized initial energy for $P = 0.1$, 0.2, and 0.3, at low B_R.

transition of cyclotron into figure-8 orbits. Little change in Δf occurs for betatron orbits.

In heating, the variance of energy, and therefore the maximum energy, $E_{\max}$, will increase with time [19]. Figure 3(a) shows $E_{\max}$ attained by an initially figure-8 orbit as a function of time for four B_R values and the same FRC parameters as in Fig. 2. $E_{\max}$ displays saturation behavior quickly, implying phase coherence growing with increasing energy. The threshold for heating is at $B_R \sim 3$ G, above which $E_{\max}$ grows $\propto B_R^{1.5}$. Figure 3(b) compares $E_{\max}$ vs B_R for figure-8 ($P = 0.22$), betatron ($P = 0.26$), and cyclotron ($P = 0.19$) orbits initiated in the $z = 0$ subspace at the same radial position, $r/R = 0.8131$, and the same energy, 1000 eV, for a simulation time of $\tau = 10^4$. Heating of figure-8 orbits occurs at lower B_R than for cyclotron or betatron orbits. At $B_R \sim 20$ G, FFTs of energy for figure-8 ions initiated at higher energy, $E > 0.031E_n \sim 30$ keV, in the $z = 0$ subspace show sharp peaks and little further gain in energy. The regular interaction of high energy figure-8 orbits with RMF$_o$ may be due to a greater separation of resonances in phase space [7,20] with increasing energy (or ω).

We have calculated the RMF$_o$-induced energy gain of a figure-8 orbit in a single half period of its motion as a first-order correction to the one-dimensional motion along r. For $P < 0.25$, the shape of the effective potential, $V(r)$, is a double well [7,21], corresponding to cyclotron orbits (in either well) inside the phase-space separatrix and to figure-8 orbits (moving across both wells) outside the phase-space separatrix. The figure-8 orbit is approximated by motion in a symmetric double well: $\rho \equiv \frac{r}{R} = \rho_0 + a_1 \cos[\omega(t - t_0)] + a_2 \cos[3\omega(t - t_0)]$, with $a_1/a_2 \sim 10$. The amplitudes of oscillation, a_1 and a_2, are determined by the total energy. The energy change from the interaction with the field is given by $dH/dt = q\vec{\mathcal{E}} \cdot \vec{v} = q(\mathcal{E}_r v_r + \mathcal{E}_\phi v_\phi)$, with $c\vec{\mathcal{E}} = -\partial\vec{A}/\partial t$. After some algebra and integrating over a single half oscillation [20,22], we get the energy gain from the interaction with the $\mathcal{E}_r$ and $\mathcal{E}_\phi$ components of the RMF. The biggest energy change occurs during a resonance, $\omega_R/\omega = s$, where s is an integer. The $\mathcal{E}_r$- and $\mathcal{E}_\phi$-induced radial and azimuthal portions of the energy change (ΔE) in a single half oscillation for an s resonance are

$$\Delta E_r = H_0\left(\sum_{n=1}^{9,n\neq s} F_n(\omega)\cos(\Psi_0) + [\hat{F}_0 + F_s]\sin(\Psi_0)\right), \quad (1)$$

$$\Delta E_\phi = H_0\left(\sum_{n=0}^{8,n\neq s} Q_n(\omega)\cos(\Psi_0) + Q_s(\omega)\sin(\Psi_0)\right), \quad (2)$$

where $F_n(\omega) = C_n[(-1)^{s+n} - 1][n/(s^2 - n^2)]$, $\hat{F}_0 = -(C_0/s)[(-1)^s - 1]$, $F_s = \frac{\pi}{2}C_s$, $Q_s(\omega) = \frac{\pi}{2}(\omega_{\rm ci}/\omega)K_s$, $Q_n(\omega) = K_n[(-1)^{s+n} - 1][s/(s^2 - n^2)](\omega_{\rm ci}/\omega)$, $\Psi_0 = \phi - \omega_R t_0$, t_0 is the initial time, $H_0 = mkR^3\omega_{\rm ci}\omega_R B_R/2B_a$, and the C_n depend on ρ_0, a_1, and a_2. Since the total energy is $H \sim \frac{1}{2}m(R\omega a_1)^2$ and $|\Omega| \sim 1$, the relative fluctuations in energy during an oscillation are of order $\max\Delta E_{\rm odd}/H \sim O(10^2 sB_R/B_a)$ and $\max\Delta E_{\rm even}/H \sim O(10s^2 B_R/B_a)$. These predict significant energy gain for figure-8 orbits over a single oscillation, even for a relatively low amplitude RMF, $B_R/B_a \sim 10^{-3}$. The energy gain for s-even resonances has an s^2 dependence while s-odd energy gain has a linear dependence on s. Resonances with an odd value of s show better heating than s-even resonances, especially at lower values of s, where the ion energy is higher. Thus, the heating observed for figure-8 orbits at higher energies results primarily from an overlap of odd-s resonances.

Using the condition for exponential separation of trajectories [22], we now determine the threshold for the ergodicity of ion trajectories, essential to convert energy gain to stochastic heating. The change in energy over an oscillation is used to map the dynamics: $E_{j+1} = E_j + \Delta E(t_j)$; $t_{j+1} = t_j + [\pi/\omega(E_{j+1})]$ where t_j is the time of the start of successive ion oscillations at $\rho = \rho_{\max} \equiv \rho_0 + a_1$ and $\Delta E(t_j)$ is $\Delta E_r(t_j) + \Delta E_\phi(t_j)$, with the substitutions $\Psi \to \Psi_j$, $\Psi_j = \phi - \omega_R t_j$, and $\Delta E \to \Delta E(t_j)$. The dynamics will be chaotic if exponential separation of trajectories, i.e., $K > 1$, occurs, where $K = \max|(dt_{j+1}/dt_j) - 1|$. In dimensionless variables, $\tilde{E} = (m/b^2R^2)E$ and $\tilde{\omega} = m\omega/b = 2\omega/\omega_{\rm ci}$, where $b = qB_a/2c$. K for odd and even resonances are

$$K_{\rm odd} \approx 8\pi s\left(\frac{1}{kR}\right)\left(\frac{B_R}{B_a}\right)\frac{d\tilde{\omega}(\tilde{E})}{d\tilde{E}}, \quad (3)$$

$$K_{\rm even} \approx \frac{\pi}{2}s^2\left(kR\right)\left(\frac{B_R}{B_a}\right)\frac{d\tilde{\omega}(\tilde{E})}{d\tilde{E}}. \quad (4)$$

Based on these, increasing the axial wave number, k, of the RMF$_o$ should lower the chaos threshold for s—odd resonances while raising the threshold for s—even resonances. This is borne out by numerical simulation.

Figure 3(c) shows $d\tilde{\omega}(\tilde{E})/d\tilde{E}$ vs $\tilde{E}$ for figure-8 orbits having $P = 0.15$. At energies very close to the separatrix,

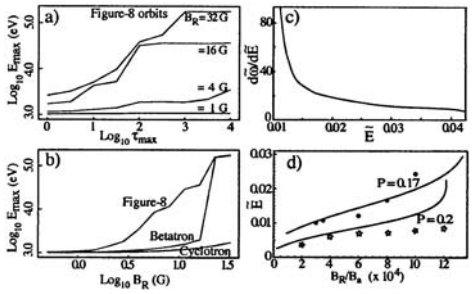

FIG. 3. (a) Maximum energy attained vs time for four values of B_R. (b) Maximum energy attained by $\tau = 10^4$ vs B_R by three types of orbits. (c) $d\tilde{\omega}(\tilde{E})/d\tilde{E}$ vs $\tilde{E}$ for figure-8 orbits; $P = 0.15$. (d) Curves: Threshold $\tilde{E}$ for saturation of stochastic heating versus B_R/B_a, based on Eqs. (3) and (4); $P = 0.17$ (upper curve) and $P = 0.2$ (lower curve); Data points, dots and stars, from RMF code.

$d\tilde{\omega}(\tilde{E})/d\tilde{E}$ grows as $(\tilde{E} - \tilde{E}_h)^{-5/6}$, where $\tilde{E}_h$ is the energy at the phase-space separatrix. The large growth of $d\tilde{\omega}(\tilde{E})/d\tilde{E}$ near the separatrix corresponds to a large increase in nonlinearity of the figure-8 orbital frequency.

The greatest rate of stochastic heating is expected to occur for lower-energy figure-8 orbits where the values of s and $d\tilde{\omega}(\tilde{E})/d\tilde{E}$ are higher. As B_R is increased, the stochastic region above the phase-space separatrix will broaden. Close to the separatrix, even very low amplitudes of B_R should produce chaotic orbits. Equations (3) and (4), combined with Fig. 3(c), can be used to estimate the relative amplitude of B_R needed to produce stochasticity and heating. For example, $s = 3$ resonance occurs at $\tilde{E} \approx .0185$, corresponding to $d\tilde{\omega}(\tilde{E})/d\tilde{E} \approx 25$; see Fig. 3(c). Using Eq. (3) and $kR \sim 1$, chaotic trajectories are to be expected for all s-odd resonances with $s \geq 3$ and $B_R/B_a \geq 5.10^{-4}$, for $\Omega \sim 1$, the assumption used in the derivation. These findings approximately agree with the numerical findings. Changing the value of a P changes the scale of $\tilde{E}$, but does not have a substantial effect on the value of $d\tilde{\omega}(\tilde{E})/d\tilde{E}$ at different resonances. Thus P determines the energy range over which figure-8 orbits get heated, with greater energy range for lower values of P, while not affecting the approximate structure of phase space. In Fig. 3(c), all $s > 4$ resonances are located to the left of $\tilde{E} \approx 0.013$, hence occur over the interval $\delta\tilde{E} \sim 0.003$. This leads to much greater chaos closer to the phase-space separatrix where the closely spaced resonances overlap. Thus, lower-energy figure-8 orbits are more chaotic and much better heated by the RMF_o than the higher energy ones. Figure 3(d) shows this effect for two values of P: 0.17 and 0.2. Figure-8 orbits are not further heated once their energy reaches (or initially exceeds) the curved line appropriate for each P value. The simplifications on which Eqs. (3) and (4) are based become less accurate at $B_R/B_a > 0.001$.

Among the clearest differences between these results for the FRC and those reported for the tokamak [15] are: (1) The nonlinearities for the FRC arise from the double potential well and field gradient and their direct effects on the particle orbit. Those in the tokamak arise from trapping in the wave field—hence require a stronger wave field—and resonance between the cyclotron motion and the wave field, resulting in a single large resonance and large first-order islands. In contrast, close spacing in phase space between resonances of a figure-8 orbit leads to an overlap between resonances and the observed stochastic heating for figure-8 orbits in FRCs. The importance of the time-varying field, $\mathcal{E}$, in the tokamak analysis is to create a small nonlinearity in this 2-D system (of the order of $\mathcal{E}/B$) which leads to resonances between the two degrees-of-freedom, not between the $\mathcal{E}$ field and the ion trajectory. (2) In the tokamak, heating occurs at 10 times higher values of Ω (over 20 vs 1 in the FRC) and lower values of $\omega_R/k\upsilon_{i,\mathrm{thermal}}$ (~ 1 vs 10). (3) The threshold for heating in the FRC is lower by the factor $sd\tilde{\omega}(\tilde{E})/d\tilde{E}$, through which the effect of the FRC's double effective-potential well is clear.

In summary, the energy gain in an orbital period due to RMF_o was calculated for a figure-8 orbit in a FRC. Resonances of ω_R with ω produce significant energy gain. Odd-s resonances more effectively heat for high-energy (lower s) figure-8 orbits. The energy gain in a oscillation was used to map the dynamics and a criterion for the exponential separation of trajectories was used to find the threshold for chaotic orbits. K, the measure of the rate of trajectory separation, increases with B_R. At higher energies, the orbits are less chaotic due to both a lower value of s and, more importantly, to a decreased nonlinearity reducing $d\tilde{\omega}(\tilde{E})/d\tilde{E}$.

This work was supported, in part, by the U.S. Department of Energy Contract No. DE-AC02-76-CHO-3073. We thank C. K. Phillips for helpful comments.

*Email address: alandsma@cantor.nrl.navy.mil

[1] T. H. Stix, *Waves in Plasmas* (American Institute of Physics, New York, 1992).
[2] M. A. Lieberman and A. J. Lichtenberg, *Principles of Plasma Discharges and Materials Processing* (John Wiley & Sons, New York, 1994).
[3] J. Chen, J. Geophys. Res. **97**, 15 011 (1992).
[4] I. Yu. Kostukov and J. M. Rax, Phys. Plasmas **7**, 185 (2000).
[5] M. Tuszewski, Nucl. Fusion **28**, 2033 (1988).
[6] J. M. Finn and R. N. Sudan, Nucl. Fusion **22**, 1443 (1982).
[7] A. S. Landsman, S. A. Cohen, M. Edelman, and G. M. Zaslavsky, Commun. Nonlinear Sci. Numer. Simul. **10**, 617 (2005).
[8] A. J. Lichtenberg and M. A. Lieberman, *Regular and Chaotic Dynamics* (Springer-Verlag, New York, 1992).
[9] W. N. Hugrass and M. Turley, J. Plasma Phys. **37**, 1 (1987).
[10] S. A. Cohen and A. H. Glasser, Phys. Rev. Lett. **85**, 5114 (2000).
[11] A. H. Glasser and S. A. Cohen, Phys. Plasmas **9**, 2093 (2002).
[12] S. A. Cohen and R. D. Milroy, Phys. Plasmas **7**, 2539 (2000).
[13] H. Y. Guo, A. L. Hoffman, R. D. Milroy, K. E. Miller, and G. R. Votroubek, Phys. Rev. Lett. **94**, 185001 (2005).
[14] C. F. F. Karney and A. Bers, Phys. Rev. Lett. **39**, 550 (1977).
[15] C. F. F. Karney, Phys. Fluids **21**, 1584 (1978).
[16] A. I. Neishtadt, V. V. Sidorenko, and D. V. Treschev, Chaos **7**, 2 (1997).
[17] A. S. Landsman, S. A. Cohen, and A. H. Glasser, Phys. Plasmas **11**, 947 (2004).
[18] Fangchuan Zhong, Yuri Petrov, and Tian-Sen Huang, Phys. Plasmas **11**, L1 (2004).
[19] M. Kac, *Probability and Related Topics in Physical Sciences* (Interscience, New York, 1958).
[20] A. S. Landsman, Ph.D. thesis, Princeton University, 2005.
[21] M. Y. Wang and G. H. Miley, Nucl. Fusion **19**, 39 (1979).
[22] G. M. Zaslavsky, *Physics of Chaos in Hamiltonian Systems* (Imperial College Press, London, 1998).